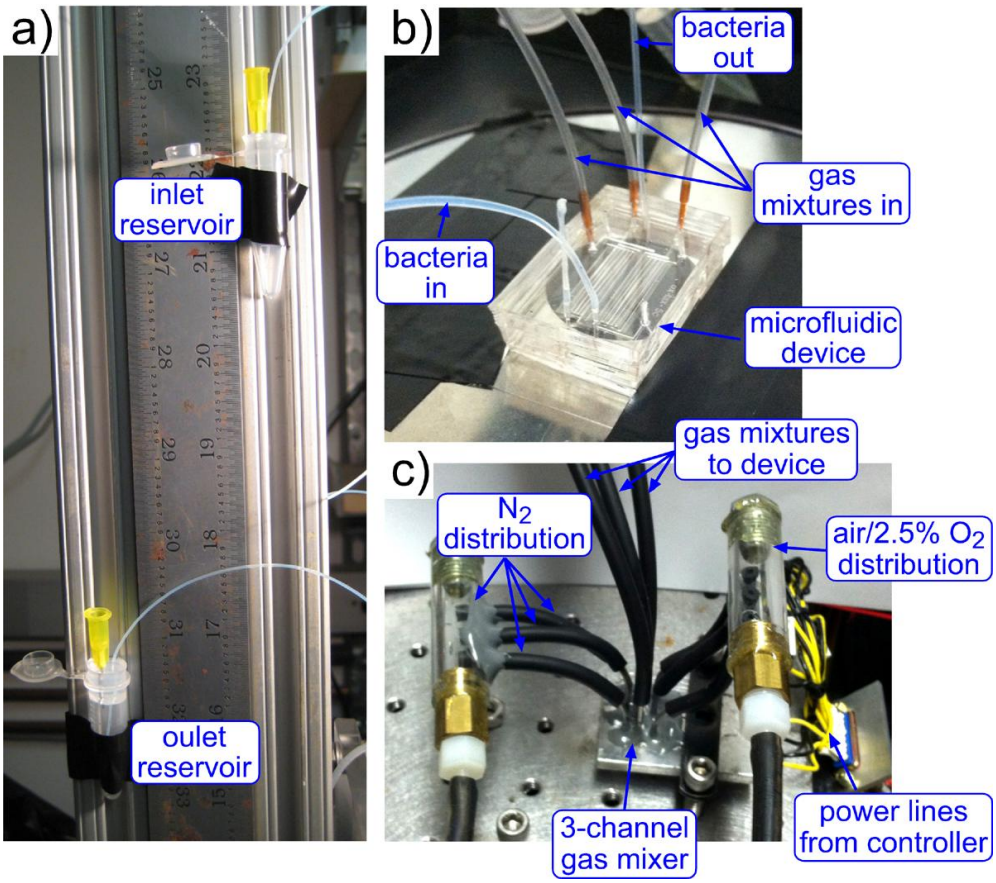

Figure S-1. Experimental setup. (a) A vertical rail with the inlet and outlet reservoirs (both made of modified Eppendorf tubes) attached to it. (b) Microfluidic device on the microscope stage with the tubing line feeding a bacterial suspension to the device (*bacteria in*, connected to the inlet reservoir), tubing line drawing the bacterial suspension from the device (*bacteria out*, connected to the outlet reservoir), and three gas tubing lines (*gas mixtures in*, connected to the 3-channel gas mixer) inserted into the inlets and outlet of the microfluidic device. (c) 3-channel gas mixer on a optical table, with different gas tubing lines and power lines connected to the mixer. The N_2 distribution unit is connected to a pressure-regulated source of N_2 and delivers compressed N_2 to the normally-open ports of the three solenoid valves of the mixer (which are situated beneath the metal board). The air/2.5% O_2 distribution unit is connected to a pressure-regulated source of either air or a mixture of 2.5% O_2 and 97.5% N_2 and delivers compressed gas to the normally-closed ports of the three solenoid valves of the mixer. The common ports of the solenoid valves are connected to the three gas inlets of the microfluidic device through the black tubing lines and *gas mixtures in* tubing lines seen in *b* (with gas mixing segments inserted in the middle[1]; not shown).

Figure S-2. Fluorescence micrographs of a segment of the gradient channel with a solution of RTDP in a PBS buffer in water taken at different $[O_2]$ in the gas channels of the microfluidic device. The field of view is 500×100 μm. The images are flat-field corrected to compensate for unevenness of the illumination and light collection. (a) $[O_2]_A = [O_2]_B = [O_2]_C = 0$ (pure N_2 in all gas channels), resulting in $[O_2] = 0$ everywhere in the gradient channel. (b) $[O_2]_A = 0$, $[O_2]_B = 20.8\%$, and $[O_2]_C = 10.4\%$, resulting in $[O_2]$ linearly varying from ~3.3% to ~17.5% across the gradient channel. (c) $[O_2]_A = [O_2]_B = [O_2]_C = 20.8$ (air in all gas channels), resulting in $[O_2] = 20.8\%$ everywhere in the gradient channel. We note that, because RTDP was dissolved in water (rather than 66% solution of ethanol in water), the ~14% variation of $[O_2]$ across the gradient channel in *b*, corresponded to a change of only ~31% in the RTDP fluorescence. Scale bar 50 μm.

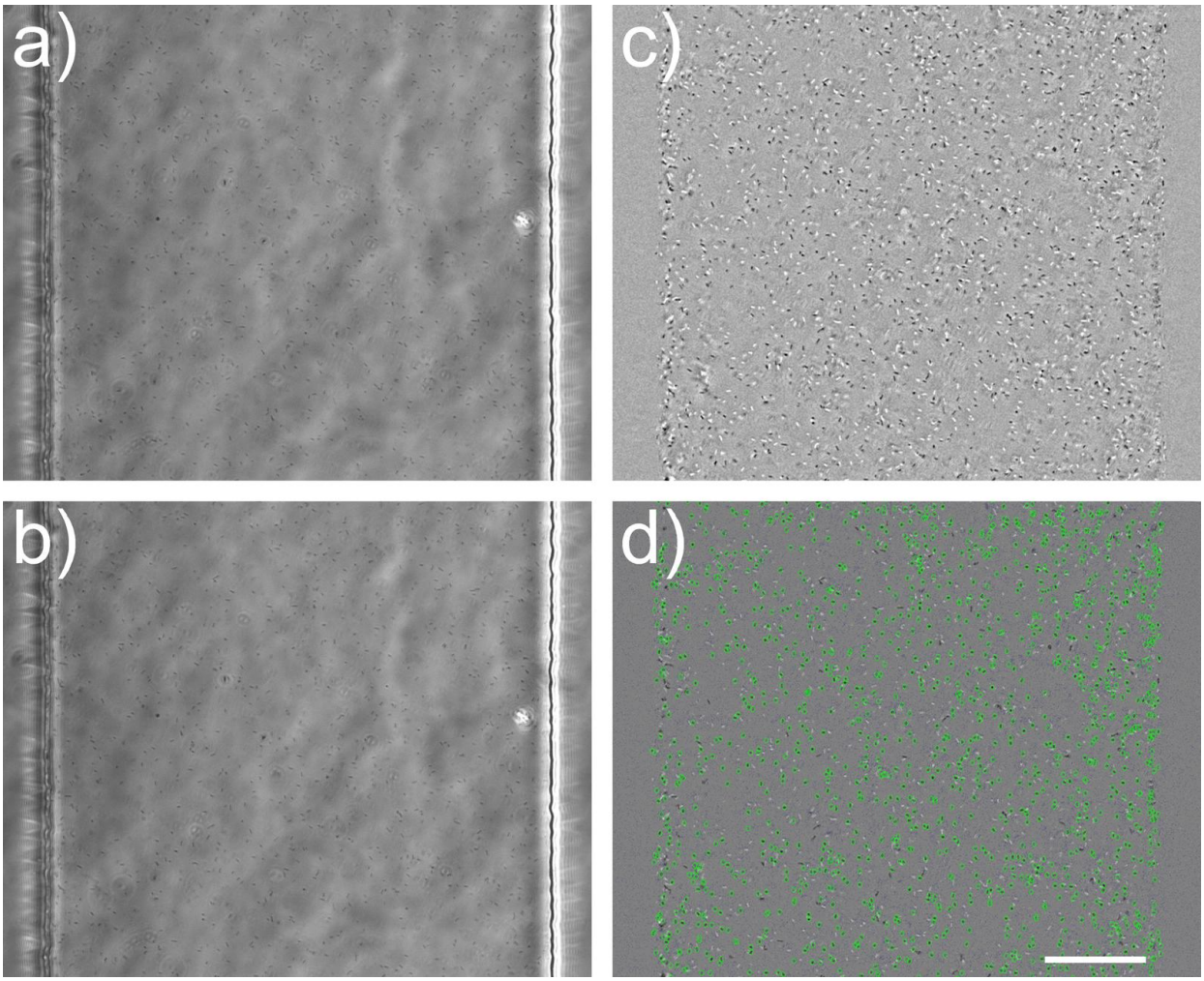

Figure S-3. Identification of individual *E. coli* cells in the gradient channel. (a) and (b) Two consecutively taken (~0.1 sec interval) brightfield micrographs of the gradient channel with *E. coli* cells at $[O_2]_A = 0$, $[O_2]_B = 1\%$, and $[O_2]_C = 0.5\%$. The micrographs were taken with a 20×/0.75 objective lens, which did not have a phase contrast ring, and to enhance the contrast, the microfluidic device was illuminated with a narrow beam directed at an angle to the vertical, resulting in visible short-range non-uniformity of illumination. (c) A result of digital processing of the images in *a* and *b*. The image in *a* was subtracted from the image in *b*; the range of the grayscales in the difference was magnified to enhance the contrast; the resulting picture was smoothened to reduce the spatially uncorrelated noise (the cumulative result of the read-out noise and shot noise due to final number of incident photons in individual pixels of the camera). As a result of the image subtraction, the high-contrast stationary features in *a* and *b* (channel side walls, a bright spot on the right, *etc*.) are suppressed in *c*, whereas moving *E. coli* cells are seen as pairs of bright and dark spots at the locations of individual cells in *a* and *b*. (d) Individual *E. coli* cells are identified using a code in Matlab that recognizes dark spots in *c* with user-defined range of sizes and with a brightness level below certain user-defined threshold. Locations of individual cells are highlighted by yellow ovals. Because the darkness/brightness and the size of the spots depend on the size of *E. coli* cells, their three-dimensional orientation, and their distance from the focal plane of the objective (which is near the mid-plane of the channel), the recognition code does not identify all cells in the field of view. Nevertheless, the identification is not biased with respect to the position across the channel, making the procedure consistent. Scale bar 100 μm.

Numerical simulations of microchannel configurations generating exponential profiles of $[O_2]$.

To generate exponential profiles of $[O_2]$, the internal edges of the in-plane gas channel networks A and B (cf. Fig. 1) are positioned asymmetrically with respect to the gradient channel, and a proper distance between the gas channel network C and the cover glass, h_g, is selected. As an example (Fig. S-4a), h_g can be reduced to 200 μm, and the distances between the edges of the 500 μm wide gradient channel and the edges of the networks A and B, Δx_A and Δx_B, can be set to 225 and 175 μm, respectively (as compared to h_g = 1.1 mm and $\Delta x_A = \Delta x_B = 100$ μm in the linear gradient device in Fig. 1a). With $[O_2]_A$ = 0, $[O_2]_B$ = 8%, and $[O_2]_C$ = 0, the resulting $[O_2]$ profile across the gradient channel is a nearly perfect exponent (blue curve in Fig. S-4d) extending over an ~50-fold range between $[O_2] \approx 0.04\%$ and 2%. The profile has a logarithmic slope $d\ln([O_2])/dx \approx 0.008\,\mu m^{-1}$, which is ~3 times greater than the representative logarithmic slope of the linear profile in the device we used for the aerotaxis experiments (Fig. 1). In another example (Fig. S-4b), with h_g = 400 μm, $\Delta x_A = 675$ μm, $\Delta x_B = 475\,\mu m$, and $[O_2]$ in the gas channels the same as before, the exponential profile extends ~7.5-fold, between $[O_2] \approx 0.45\%$ and 3.4%, with a logarithmic slope of ~0.004 μm^{-1} (a factor of ~1.5 greater than in the device in Fig. 1; red curve in Fig. S-4d). In a third example (Fig. S-4c), with h_g = 800 μm, $\Delta x_A = 950$ μm, $\Delta x_B = 550\,\mu m$, the exponential profile extends ~2.9-fold, between $[O_2] \approx 1.39\%$ and 4.03% with a logarithmic slope of ~0.002 μm^{-1} (green curve in Fig. 6d).

The results of the simulations (Fig. S-4) show that, with a proper selection of the three geometrical parameters, h_g, Δx_A, and Δx_B, exponential profiles of $[O_2]$ with a range of logarithmic slopes can be generated. It is worth noting, however, that exponential profiles with large logarithmic slopes require small h_g, making the gradient channel less structurally stable (more flexible roof). Also, the shapes of the profiles generated by the devices in Fig. S-4a-c as well as the values of $[O_2]$ at given x are substantially more dependent on h_g, as compared to the device in Fig. 1. Therefore, the casting of the PDMS chips for the devices in Fig. S-4a-c would need to be controlled more rigorously.

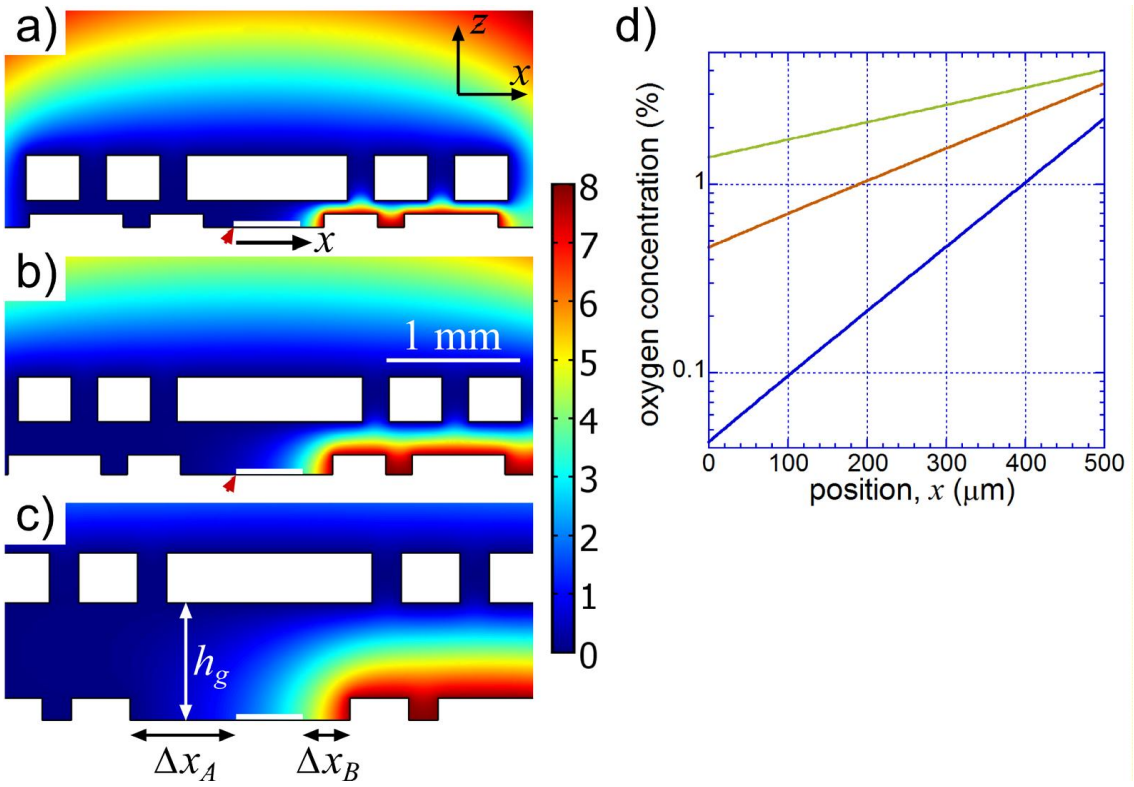

Figure S-4. Two-dimensional numerical simulations of PDMS chips generating exponential profiles of $[O_2]$ in a liquid-filled gradient channel. (a) – (c) Color-coded distributions of $[O_2]$ in bottom-central areas of *xz*-cross-sections of chips with different gas channel layouts (cf. Fig. 1b). The color legend is shown by a bar on the right with numbers indicating $[O_2]$ in percents. 500 μm wide gradient channels are shown by white strips at the center bottom of each panel, with their left edges marked by red arrows. The computational domain is 20×5 mm in the *xz*-plane, with an impermeable boundary at the bottom (cover glass) and $[O_2]$ = 20.8% at the top and on the sides. In all three cases, $[O_2]$ is 0 in the in-plane gas channels to the left from the gradient channel (network A) and in the out-of-plane gas channels (network C) and 8% in the in-plane gas channels to the right from the gradient channels (network B). The distances between the cover glass and out-of-plane gas channels, h_g, are 200, 400, and 800 μm in *a*, *b*, and *c*, respectively. (d) Oxygen concentration, $[O_2]$, across the gradient channels for the devices in *a* (blue line), *b* (red line), and *c* (green line) in semi-logarithmic coordinates. In all three cases, the lines are visually indistinguishable from exponential fits. The exponents, $d\ln([O_2])/dx$, are ~0.008, ~0.004, and ~0.002 μm^{-1} for the blue, red, and green lines, respectively.

(1) Adler, M.; Polinkovsky, M.; Gutierrez, E.; Groisman, A. *Lab On A Chip* **2010**, *10*, 388-391.